CHEMISTRY OF MATERIALS

Article

pubs.acs.org/cm

Mechanistic Roles of Hydroxide in Controlling the Deposition of Gold on Colloidal Silver Nanocrystals

Xiaojun Sun,[†] Yin Yang,[†,‡] Zhiwei Zhang,[†] and Dong Qin*[,†]

[†]School of Materials Science and Engineering, Georgia Institute of Technology, Atlanta, Georgia 30332, United States

[‡]Institute of Advanced Synthesis, School of Chemistry and Molecular Engineering, Jiangsu National Synergetic Innovation Center for Advanced Materials, Nanjing Tech University, Nanjing 211816, P. R. China

Supporting Information

ABSTRACT: This article describes a systematic study of the roles played by hydroxide in controlling the deposition of Au on Ag nanocubes for the fabrication of diversified Ag–Au bimetallic nanocrystals. The synthesis simply involves the titration of aqueous $HAuCl_4$ into an aqueous suspension of Ag nanocubes in the presence of ascorbic acid (H_2Asc), NaOH, and poly(vinylpyrrolidone) at room temperature. The OH^- ions from NaOH can affect the reduction kinetics of the Au(III) precursor in a number of ways and thereby the deposition pathways of the Au atoms. First of all, the OH^- can accelerate the reduction kinetics by neutralizing H_2Asc into ascorbate monoanion ($HAsc^-$), the true player behind the reduction power of ascorbic acid. Second, the OH^- can neutralize the added $HAuCl_4$ and progressively transform $AuCl_4^-$ into $AuCl_3(OH)^-$, $AuCl_2(OH)_2^-$, $AuCl(OH)_3^-$, or $Au(OH)_4^-$ through ligand exchange, generating Au(III) precursors with increasingly lower reduction potentials and thus lower probability for galvanic replacement reaction with Ag nanocubes than $AuCl_4^-$. Third, the OH^- can react with the Ag^+ ions released from the galvanic reaction to generate Ag_2O patches at the corners of Ag nanocubes. Our results indicate that the deposition of Au on Ag nanocubes can follow two distinct pathways depending on the initial pH of the reaction solution. When the initial pH is controlled in the range of 10.3–11.9, the reduction of Au(III) is initiated by Ag nanocubes but dominated by $HAsc^-$ afterward, leading to the formation of Ag@Au core-frame and then core–shell nanocubes. In contrast, if the initial pH is controlled in the range of 3.2–4.8, both the galvanic replacement with Ag nanocubes and the chemical reduction by $HAsc^-$ contribute to the conversion of Au(III) to Au atoms. The Ag^+ ions released from the galvanic replacement can also be reduced by $HAsc^-$ to transform Ag nanocubes into Ag@Ag–Au concave nanocubes with hollow interiors and alloyed walls.

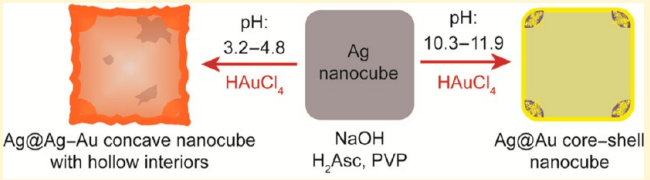

INTRODUCTION

Silver nanocrystals have been actively explored for a variety of applications including those related to localized surface plasmon resonance (LSPR),[1−3] surface-enhanced Raman scattering (SERS),[4−7] colorimetric sensing,[8,9] and catalysis/photocatalysis.[10,11] Despite the large number of demonstrations, the ultimate performance of Ag nanocrystals is often compromised by their shape instability under an oxidative environment. In the case of Ag nanocubes, for example, the atoms located at corners and edges could be readily oxidized to Ag^+ ions, which result in the transformation of shape and thus the deterioration of SERS activity.[12] On the other hand, while Ag has remarkable catalytic properties for oxidation reactions such as ethylene epoxidation,[11,13] its capability toward reduction reactions tends to be compromised when compared with other noble metals such as Pd and Pt.

One strategy to expand the application landscape of Ag nanocrystals is to introduce another noble metal (M) such as Au, Pd, or Pt to generate diversified and yet well-defined Ag-M bimetallic nanocrystals. For example, conformally coating the surface of Ag nanocubes with ultrathin shells made of Au could greatly improve their chemical stability under a corrosive environment.[14,15] Selective deposition of Pd atoms on the edges of Ag nanocubes has been demonstrated for the fabrication of Ag@Pd core-frame nanocubes that exhibit a combination of catalytic activities toward both oxidation and reduction reactions.[16−18] In particular, the presence of Ag in the cores of these nanostructures has led to the development of bifunctional probes capable of reporting the catalytic reactions in situ by SERS. In developing these advanced bimetallic nanocrystals, it is critical to be able to defeat the galvanic replacement reaction between the Ag nanocrystals and a precursor to M atoms.[14,19] Also, it is pivotal to control the sites at which the newly formed M atoms will be deposited.

Seed-mediated growth offers a powerful route to the aforementioned bimetallic nanocrystals. In a typical synthesis, Ag nanocrystals (the seeds) are dispersed in an aqueous solution containing ascorbic acid (H_2Asc, a forerunner of the reducing agent) and poly(vinylpyrrolidone) (PVP, a colloidal stabilizer), followed by the titration of a precursor solution. However, the capability of this approach is limited by galvanic replacement when the metal M is less reactive than Ag. The

Received: February 10, 2017
Revised: April 17, 2017
Published: April 18, 2017

ACS Publications © XXXX American Chemical Society

DOI: 10.1021/acs.chemmater.7b00575
Chem. Mater. XXXX, XXX, XXX−XXX

involvement of galvanic replacement will make it difficult to control the outcome of seeded growth and even cause degradation to the properties associated with the nanocrystals. To suppress the galvanic replacement, for example, between Au(III) and Ag, we demonstrated that it was essential to increase the pH of the reaction solution to a level above 11.2 by introducing NaOH.[14] Our hypothesis was that the Au(III) precursor would be reduced by ascorbic acid exclusively before they could undertake galvanic replacement with Ag, leading to the generation of Au atoms for their conformal deposition on the Ag nanocrystals.[14] Despite the successful synthesis of Ag@Au core−shell nanocubes with a shell thickness controlled at three or six atomic layers, we were unable to pin down the mechanistic roles played by the NaOH added into the reaction system.

From the perspective of chemical reactions, the OH^- ions can serve a number of different roles in a typical synthesis of Ag−Au bimetallic nanocrystals. First, H_2Asc is a weak diprotic acid with dissociation constants of $pKa_1 = 4.2$ and $pKa_2 = 11.6$, respectively, at 25 °C.[20] According to literature, it is the ascorbate monoanion ($HAsc^-$), rather than the parental acid (H_2Asc), that can donate electrons and thus act as a reducing agent (Figure S1).[20] The dissociation equilibrium of H_2Asc into $HAsc^-$ and H^+ can be pushed to the right side as more OH^- is introduced, which leads to a higher concentration for $HAsc^-$, the actual reducing agent. The increasingly accelerated reduction of the Au(III) precursor by $HAsc^-$ can eventually suppress the galvanic replacement reaction with the Ag nanocrystals. Second, it is well-established that $AuCl_4^-$ can progressively evolve into a series of complexes, including $AuCl_3(OH)^-$, $AuCl_2(OH)_2^-$ $AuCl(OH)_3^-$, and $Au(OH)_4^-$, through ligand exchange with OH^-.[21] In this case, the reduction potential of the Au(III) precursor will decrease when moving from $AuCl_4^-$ to $Au(OH)_4^-$, slowing down the reduction by both the $HAsc^-$ and the galvanic reaction.[22] Last but not least, the presence of Ag^+ ions (e.g., released from the possible galvanic reaction) and OH^- in the same reaction solution can result in the formation of Ag_2O, an oxide insoluble in an alkaline solution but soluble in an acidic solution.[23] When deposited on the Ag nanocrystals, the Ag_2O patches can mediate the dissolution behavior of Ag as well as the deposition pattern of Au.

Herein, we report a systematic study aiming to elucidate the explicit roles played by OH^- in controlling the pathways responsible for the transformation of Ag nanocubes into diversified Ag−Au bimetallic nanostructures. In a typical process, we dispersed Ag nanocubes in an aqueous solution containing H_2Asc, NaOH, and PVP, followed by the titration of aqueous $HAuCl_4$ using a syringe pump at room temperature. By introducing different amounts of NaOH prior to the titration of $HAuCl_4$, we could easily adjust the initial pH of the reaction solution from 3.2 to 11.9. After a set of survey experiments, we specifically focused on two conditions with the initial pH adjusted to 11.9 and 4.8, respectively. At an initial pH of 11.9, the reaction solution could be maintained alkaline (pH = 11.9−10.0) during the titration of aqueous 0.1 mM $HAuCl_4$ up to 0.8 mL. In this case, the H_2Asc was neutralized by NaOH to generate $HAsc^-$, while the added $HAuCl_4$ was also quickly neutralized by OH^- to yield $AuCl_4^-$. For the first few drops of precursor solution, the $AuCl_4^-$ could still be reduced by Ag nanocubes through the galvanic replacement reaction before it underwent ligand exchange with OH^-. In this case, the Ag atoms were oxidized and dissolved from the corners while the resultant Au atoms were deposited on the edges of the Ag nanocubes. The released Ag^+ ions immediately reacted with the surrounding OH^- for the formation of Ag_2O patches at the corners, blocking the underlying Ag from further dissolution. Meanwhile, $AuCl(OH)_3^-$ and $Au(OH)_4^-$, both with lower reduction potentials than that of $AuCl_4^-$, were formed through ligand exchange with OH^-. These Au(III) species were quickly reduced by $HAsc^-$ for the production of Au atoms, followed by their sequential deposition on the edges and side faces, leading to the generation of Ag@Au core-frame and then core−shell nanocubes. At an initial pH of 4.8, the reaction solution could be maintained acidic (pH = 4.8−4.6) during the titration of aqueous 0.1 mM $HAuCl_4$ up to 0.8 mL. In this case, only some of the added H_2Asc was neutralized by NaOH to yield $HAsc^-$, slowing down the reduction kinetics. The added $HAuCl_4$ could still be neutralized to generate $AuCl_4^-$, which then evolved into $AuCl_3(OH)^-$ and $AuCl_2(OH)_2^-$ through ligand exchange. All these Au(III) species could undergo galvanic replacement with Ag nanocubes. However, the released Ag^+ ions could not be converted to Ag_2O under an acidic condition, and instead, they were reduced to Ag atoms by $HAsc^-$ and codeposited with Au atoms on the Ag nanocubes. As a result, the Ag nanocubes were transformed into Ag@Ag−Au concave nanocubes with hollow interiors and alloyed walls.

EXPERIMENTAL SECTION

Chemicals and Materials. Silver trifluoroacetate (CF_3COOAg, 98%), gold(III) chloride trihydrate ($HAuCl_4{\cdot}3H_2O$, 99.9+%), sodium hydrosulfide hydrate ($NaHS{\cdot}xH_2O$), aqueous hydrochloric acid (HCl, 37%), PVP with an average molecular weight of 29 000 (PVP-29k) or 55 000 (PVP-55k), L-ascorbic acid (H_2Asc, 99%), sodium hydroxide (NaOH, 98+%), and hydrogen peroxide (H_2O_2, 30 wt % in H_2O) were all acquired from Sigma-Aldrich. Ethylene glycol (EG) was purchased from J. T. Baker. All chemicals were used as received. All the aqueous solutions were prepared using deionized (DI) water with a resistivity of 18.2 MΩ cm at room temperature. The aqueous solutions of $HAuCl_4$ and NaOH used in the present work were 0.1 mM and 0.2 M, respectively, in molar concentration, unless otherwise specified in the text.

Synthesis of Ag Nanocubes. We prepared Ag nanocubes with an edge length of 38.6 ± 1.3 nm by following the protocol developed by Xia and co-workers.[24] After precipitation with acetone, the nanocubes were collected by centrifugation at 6500 rpm for 5 min, washed with DI water three times, and then dispersed in water for storage and further use. Figure S2 shows typical scanning electron microscopy (SEM) and transmission electron microscopy (TEM) images of the Ag nanocubes.

Synthesis of Ag−Au Bimetallic Nanocubes. In a standard protocol, 2 mL of aqueous PVP-29k (1 mM) was added into a 23 mL glass vial, followed by the introduction of 0.5 mL of aqueous H_2Asc (0.1 M) and a specific volume (0.1, 0.2, 0.3, 0.4, 0.5 mL) of aqueous NaOH (0.2 M). After mixing under magnetic stirring, we pipetted 19 μL of the aqueous suspension of Ag nanocubes into the mixture with a final concentration of 4.2×10^{10} particles/mL. Afterward, aqueous $HAuCl_4$ (0.1 mM) was titrated into the mixture using a syringe pump at a rate of 0.02 mL/min at room temperature. The reaction solution was maintained for another 10 min once the titration was completed. The products were collected by centrifugation at 6500 rpm for 12 min, washed twice with water, and then dispersed in water for further characterization.

Selective Etching of Ag from the Ag@Ag Core−Shell Nanocubes. We incubated the as-prepared sample in a solution containing 0.7 mL of PVP-29k (1 mM) and 0.3 mL of H_2Asc (0.1 M) at room temperature for 10 min. The particles were then collected by centrifugation at 6000 rpm for 12 min, followed by redispersion in 0.1 mL of water. We then introduced 1 mL of 3% H_2O_2, and the etching was allowed to proceed for 2 h. The final products were collected by

DOI: 10.1021/acs.chemmater.7b00575
Chem. Mater. XXXX, XXX, XXX−XXX

centrifugation at 13 000 rpm for 18 min, followed by washing twice with water and redispersion in water for further characterization.

Selective Etching of Ag from Ag@Ag−Au Concave Nanocubes. We redispersed as-obtained sample in 0.1 mL of DI water at room temperature. We then introduced 1 mL of 3% H_2O_2, and the etching was allowed to proceed for 2 h. The final products were collected by centrifugation at 13 000 rpm for 18 min, followed by washing twice with water and redispersion in water for further characterization.

Analyzing the Galvanic Replacement Reaction between Ag Nanocubes and $HAuCl_4$ in the Absence and Presence of NaOH. In the absence of NaOH, we pipetted 2 mL of aqueous PVP-29k (1 mM) to 0.5 mL of water in a 23-ml glass vial, and the pH was 4.3 for the reaction solution. To adjust the pH to 11.4, we prepared the aqueous reaction solution by introducing 2 mL of PVP-29k (1 mM), 0.06 mL of NaOH (0.2 M), and 0.44 mL of water to a 23-mL glass vial. In each case, 19 μL of the aqueous suspension of Ag nanocubes was introduced, followed by the titration of 0.2, 0.4, 0.6, and 0.8 mL of aqueous $HAuCl_4$ (0.1 mM) using a syringe pump at a rate of 0.02 mL/min at room temperature. After the completion of titration, we waited for 10 min and then collected both solid and supernatant for inductively coupled plasma mass spectrometry (ICP-MS) measurements to determine the Au and Ag contents in each sample.

Instrumentation and Characterization. We collected the samples using Eppendorf 5430 (Eppendorf North America, Hauppauge, NY). The pH value was measured using a FiveEasy pH Meter (Mettler Toledo, Columbus, OH). The UV−vis spectra were collected using a Cary 50 spectrometer (Agilent Technologies, Santa Clara, CA). TEM images were taken using a Hitachi HT7700 microscope (Hitachi, Tokyo, Japan) operated at 120 kV. SEM images were captured using a Hitachi SU-8230 microscope operated at 20 kV. The contents of Au and Ag were determined using ICP-MS on NexION 300Q (PerkinElmer, Waltham, MA).

RESULTS AND DISCUSSION

We started with the preparation and characterization of aqueous suspensions containing the same amount of Ag nanocubes, H_2Asc, and PVP, but different amounts of NaOH. As shown in Figure 1A, the pH value of the reaction solution containing 0.5 mL of 0.1 M H_2Asc increased from 3.2 to 4.1, 4.8, 10.3, 11.5, and 11.9 when 0.1, 0.2, 0.3, 0.4, and 0.5 mL of 0.2 M aqueous NaOH was added, respectively. This is a typical curve when a weak acid is titrated with a strong base. Ascorbic acid is a weak diprotic acid, with *p*Ka at 4.2 and 11.6, respectively.[20] After the addition of 0.25 mL of NaOH solution, the reaction solution (pH = 7.2) should be dominated by ascorbate monoanion ($HAsc^-$) as all the H_2Asc (0.05 mmol) in the system should have been neutralized by the OH^- according to the following reaction:

$$H_2Asc + OH^- = HAsc^- + H_2O \quad (1)$$

According to literature, it is $HAsc^-$, not H_2Asc, that can donate electrons and serve as a reducing agent (Figure S2).[20] As such, we expect that the reducing power of the same aqueous solution of H_2Asc will differ significantly when its pH is adjusted to the alkaline and acidic regions because of the large difference in $HAsc^-$ concentration. The difference in reduction kinetics, in turn, would lead to the formation of distinct products when Ag nanocubes are reacted with $HAuCl_4$ in an aqueous system, as observed in our previous studies.[14,25]

In the initial survey experiments, we employed UV−vis spectroscopy to compare the LSPR properties of the Ag nanocubes before and after reacting with 0.4 mL of 0.1 mM aqueous $HAuCl_4$ titrated into the reaction solutions with different initial pH values. As shown in Figure 1B, when the initial pH was controlled at 3.2, 4.1, and 4.8, the major LSPR

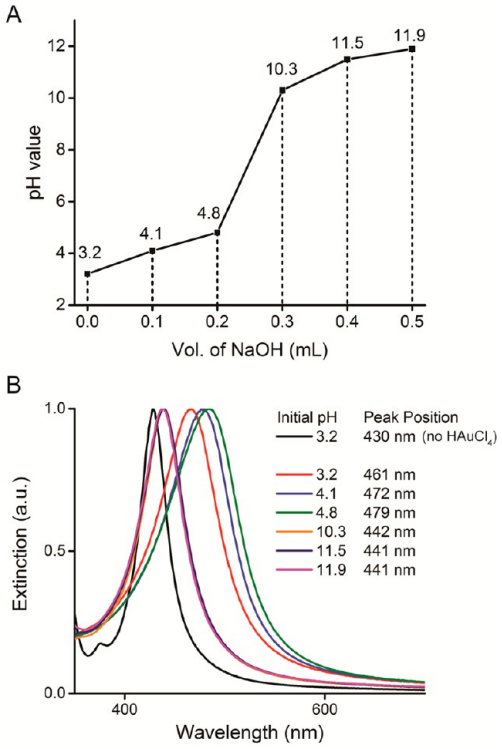

Figure 1. (A) pH value of a reaction solution as a function of the volume of 0.2 M aqueous NaOH added without the titration of aqueous $HAuCl_4$. (B) UV−vis spectra of Ag nanocubes before and after reacting with 0.4 mL of 0.1 mM aqueous $HAuCl_4$ at six different initial pH values for the reaction solutions.

peak of the Ag nanocubes was notably shifted from 430 to 461, 472, and 479 nm, respectively. These results suggest that the reaction with $HAuCl_4$ caused major structural or morphological changes to the Ag nanocubes when the reaction solution was acidic, with an initial pH in the range of 3.2−4.8. In comparison, if the initial pH was tuned to 10.3, 11.5, and 11.9, the major LSPR peak of the Ag nanocubes only showed slight shift from 430 to 442, 441, and 441 nm, respectively. The insignificant shift in peak position indicates that the structure or morphology of the parental Ag nanocubes was largely preserved during the titration of $HAuCl_4$ when the reaction solution was alkaline, with an initial pH in the range of 10.3−11.9.

We then used electron microscopy to characterize the products obtained upon the titration of 0.4 mL of 0.1 mM $HAuCl_4$ solution in the presence of different amounts of NaOH and thus different initial pH values. Figure 2 shows SEM and TEM images of the as-obtained products. At an initial pH of 3.2 (i.e., without adding any NaOH), the products exhibited slightly sharpened edges in addition to the observation of small pits on the surface (Figure 2A). The TEM image in Figure 2B confirms the presence of voids in most of the nanocubes. The formation of voids can be attributed to the involvement of galvanic replacement reaction between the Ag nanocubes and the Au(III) precursor titrated into the reaction solution. The released Ag^+ ions and the titrated Au(III) precursor were both reduced to atoms for their codeposition onto the edges of the nanocubes, and as a result, their edges appeared to be sharpened, consistent with our previous findings.[25] When the initial pH was increased to 4.1 by adding 0.1 mL of the aqueous NaOH, the products also exhibited sharpened edges and corners, but with fewer voids and increased concaveness for the

DOI: 10.1021/acs.chemmater.7b00575
Chem. Mater. XXXX, XXX, XXX−XXX

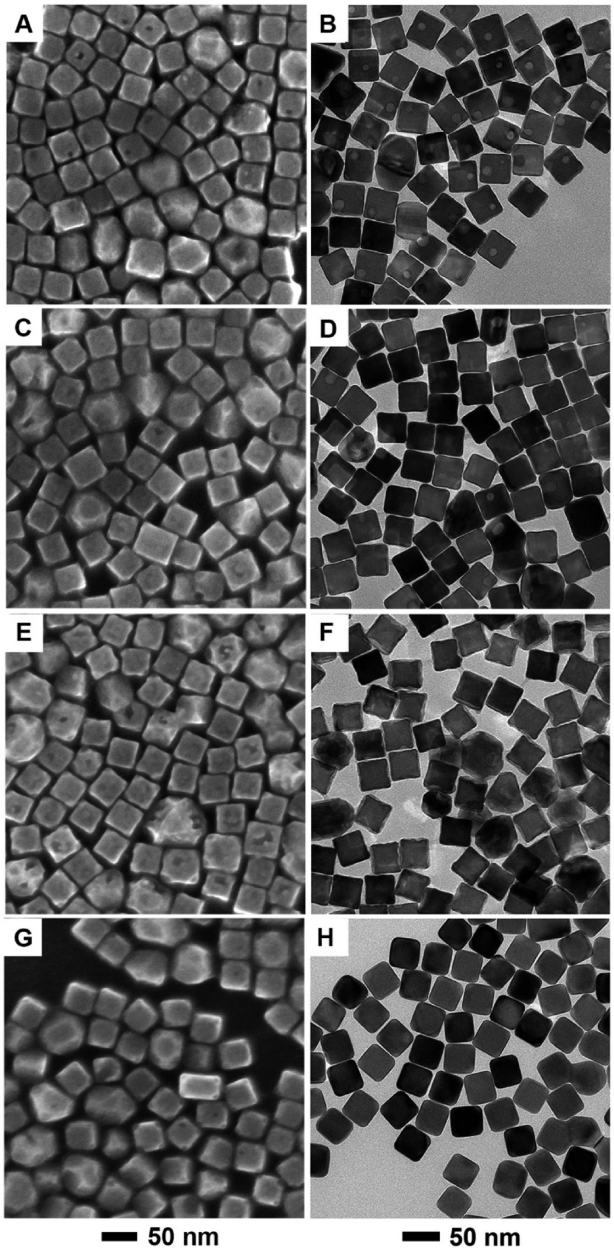

Figure 2. SEM (left panel) and TEM (right panel) images of Ag nanocubes after reacting with 0.4 mL of 0.1 mM aqueous $HAuCl_4$ at different initial pH values for the reaction solutions: (A, B) 3.2, (C, D) 4.1, (E, F) 4.8, and (G, H) 11.9, respectively.

side faces (Figure 2C,D). This observation suggests that the galvanic replacement reaction was retarded to a certain extent with the addition of NaOH. The increase in concaveness indicates that more atoms were preferentially deposited on the edges of the nanocubes. It is worth mentioning that the increase in concaveness could also contribute to the significant red-shift of the LSPR peak to 472 nm. When the initial pH was further increased to 4.8 by introducing 0.2 mL of the aqueous NaOH, the SEM image indicates that the particles started to take a rough surface and more concave shape (Figure 2E), consistent with the observation of wavy edges observed under TEM (Figure 2F). The TEM image indicates the absence of voids in the nanocubes. In this case, the galvanic reaction was further suppressed because of the increase in initial pH. Again, the codeposition of Au and Ag atoms on the edges gave rise to nanocubes with a concave shape, supporting the red-shift of LSPR peak position to 479 nm. When the initial pH of the reaction solution was further increased to the alkaline region with a pH of 11.9 by adding 0.5 mL of the aqueous NaOH, the as-obtained particles exhibited a morphology similar to the parental Ag nanocubes, except for slight truncation at the corner sites (Figure 2G,H). Under this circumstance, there was essentially no involvement of galvanic replacement reaction and the Au(III) precursor was reduced to Au atoms for their conformal deposition on the edges and side faces. The as-obtained particles showed an LSPR peak at 441 nm, which closely resembled that of the original Ag nanocubes at 430 nm.

According to the outcomes of the survey experiments, the reaction can be divided into two major groups, corresponding to alkaline and acidic conditions, respectively. As such, we decided to focus on the products obtained by titrating different volumes of aqueous $HAuCl_4$ into aqueous suspensions of Ag nanocubes with an initial pH in the alkaline and acidic regions, respectively. In the first set of experiments, we introduced 0.5 mL of the aqueous NaOH into a mixture of Ag nanocubes, H_2Asc, and PVP to attain an initial pH of 11.9, followed by the titration of different volumes of the aqueous $HAuCl_4$. As shown in Figure S3A, the pH of the reaction solution gradually decreased from 11.9 to 10.0 during the introduction of 0.8 mL of aqueous $HAuCl_4$ due to its acidic characteristic (pH = 4.0 for a 0.1 mM aqueous solution). Within this pH range, the solution of H_2Asc should be dominated by $HAsc^-$. Figure 3, A, C, and E show typical TEM images of the samples obtained at titration volumes of 0.2, 0.4, and 0.8 mL, respectively, for the $HAuCl_4$ solution. We noticed that their morphology was very similar to that of the original Ag nanocubes, except for an increase in edge length from 38.6 ± 1.3 nm to 38.9 ± 1.7 nm, 39.3 ± 1.6 nm, and 40.3 ± 1.9 nm, respectively. To reveal the distribution of Au atoms on the surface of Ag nanocubes, we used 3% aqueous H_2O_2 to selectively remove Ag while leaving Au intact. Following one of our recently established protocols,[26] we collected aliquots of samples shown in Figure 3, A, C, and E and incubated them in an aqueous solution containing PVP-29k and H_2Asc for 10 min. The treated samples were then collected by centrifugation and etched in 3% H_2O_2. As shown in Figure 3B, nanoframes with pores at corners and sizes slightly smaller than the original nanocubes were formed upon the removal of Ag cores from the sample obtained with the titration of 0.2 mL of aqueous $HAuCl_4$. The nanoframes shrank in dimensions relative to the original nanocubes because they were not rigid enough to sustain the sample drying process. The small openings at the corners confirm that the Au atoms were preferentially deposited on the edges of the nanocubes with the corners largely uncovered. At 0.4 mL, the TEM image in Figure 3D shows that nanocages with pores at the corners and side faces were obtained after the removal of Ag cores. In this case, the Au atoms were deposited on the edges and side faces of the nanocubes for the generation of Ag@Au core−shell nanocubes. The integrity of the Au layer on side faces was compromised by the inadequate amount of $HAuCl_4$, and as a result, there were pores on the side faces after the removal of Ag template. The TEM image in Figure 3F shows the formation of nanoboxes with well-defined pores at the corner sites after the removal of Ag cores from the sample obtained with the addition of 0.8 mL of $HAuCl_4$. By comparing with the conventional nanocages reported in literature,[27] the nanoboxes exhibited well-defined openings at the corner sites and continuous side faces, which suggested that the Au atoms were continuously deposited on

DOI: 10.1021/acs.chemmater.7b00575
Chem. Mater. XXXX, XXX, XXX−XXX

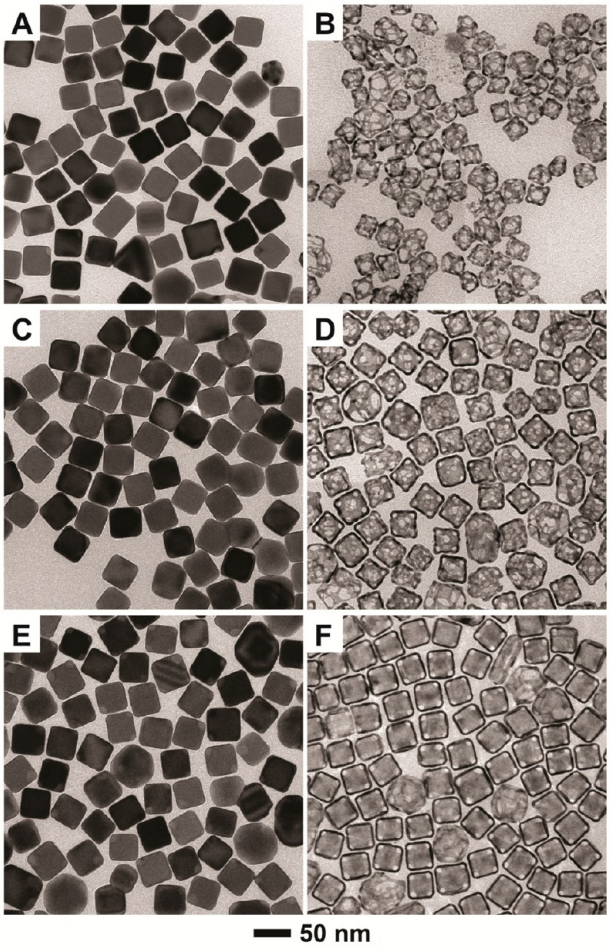

Figure 3. TEM images of products before (left panel) and after (right panel) treatment with H_2Asc and then 3% aqueous H_2O_2. The samples were prepared at an initial pH of 11.9 by titrating different volumes of 0.1 mM aqueous $HAuCl_4$: (A, B) 0.2, (C, D) 0.4, and (E, F) 0.8 mL, respectively.

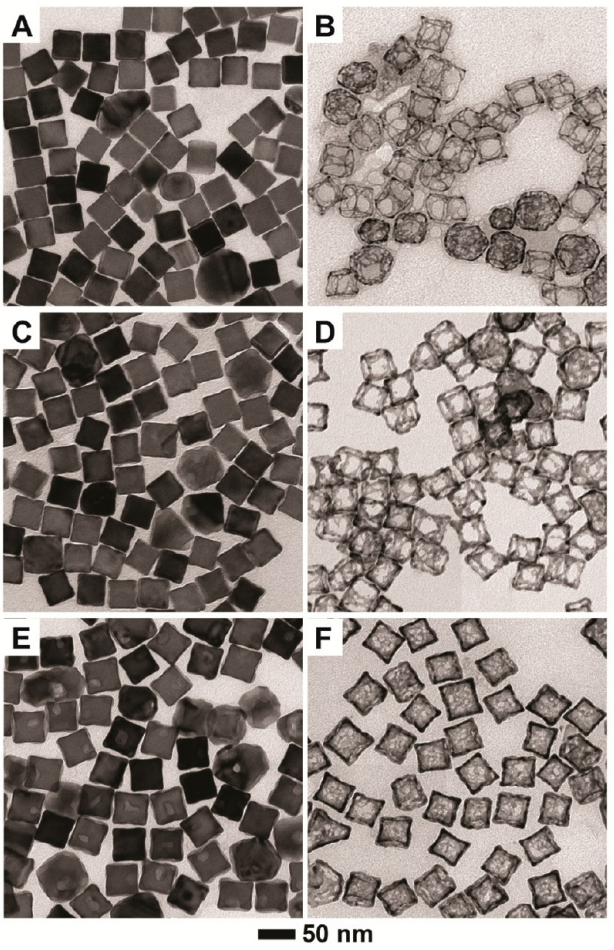

Figure 4. TEM images of products before (left panel) and after (right panel) treatment with 3% aqueous H_2O_2. The samples were prepared at an initial pH of 4.8 by titrating different volumes of 0.1 mM aqueous $HAuCl_4$: (A, B) 0.2, (C, D) 0.4, and (E, F) 0.8 mL, respectively.

the side faces for the formation of thicker Au shells that could survive the etching process.

In another set of experiments, we performed a parallel study by adding 0.2 mL of the NaOH solution to attain an initial pH of 4.8 while keeping all the other parameters the same as in Figure 3. As shown in Figure S3B, the pH of the reaction solution was slightly decreased from 4.8 to 4.6 with the addition of 0.1 mM aqueous $HAuCl_4$ up to 0.8 mL. Figure 4 shows TEM images of the samples obtained after adding different volumes of the $HAuCl_4$ solution and the corresponding structures after H_2O_2 etching. At a titration volume of 0.2 mL, we observed the transformation of Ag nanocubes into nanocubes with sharpened corners (Figure 4A) and then cubic nanoframes upon the removal of Ag cores (Figure 4B). Some nanoframes exhibited pores at the corners while the edges were slightly distorted due to the lack of rigidity. When the volume of $HAuCl_4$ solution was increased to 0.4 and 0.8 mL, we noticed that more Au atoms were accumulated at the corners and edges, together with more pronounced surface roughness and surface concaveness, and void formation (Figure 4C,E). These results support our argument that Ag could be continuously oxidized through the galvanic replacement reaction with Au(III) in an acidic solution. The released Ag^+ ions together with Au(III) were then reduced into atoms, followed by their deposition on the edges and corners of the Ag nanocubes. During the etching of Ag cores and the dealloying of Ag from their walls, the structures evolved into nanocages with decreasing porosity on the side faces (Figure 4D,F). These results also suggest that the deposited Au and Ag atoms could migrate from edges and corners to the side faces as more precursor was introduced.

We also characterized the LSPR properties of the Ag nanocubes before and after reacting with different amounts of $HAuCl_4$ in the presence of 0.5 and 0.2 mL of the aqueous NaOH, respectively, to give initial pH values of 11.9 and 4.8. As shown in Figure 5A, the major LSPR peak was only shifted from 430 to 445 nm in the case of an initial pH of 11.9, consistent with the argument that the Au atoms are conformally deposited on the surface of Ag nanocubes without involving galvanic replacement reaction. In contrast, at an initial pH of 4.8, the major LSPR peak of the Ag nanocubes was significantly shifted from 430 to 512 nm, as shown in Figure 5B. This result can be attributed to the presence of pits/voids formed through the galvanic replacement reaction and the increase in concaveness due to the preferential deposition of Au and Ag atoms on the edges.

On the basis of the experimental results presented in Figures 3 and 4, we propose two scenarios to account for the reaction involving $HAuCl_4$, H_2Asc, and Ag nanocubes at pH initially

DOI: 10.1021/acs.chemmater.7b00575
Chem. Mater. XXXX, XXX, XXX−XXX

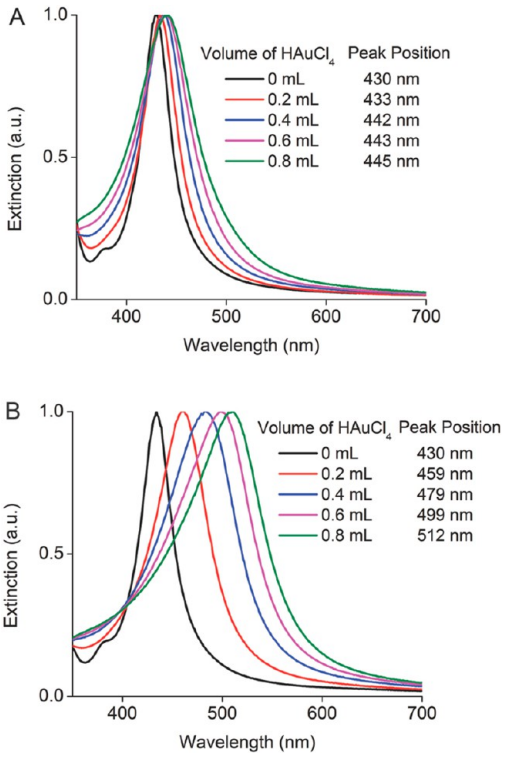

Figure 5. UV−vis spectra recorded from suspension of the Ag nanocubes after reacting with different volumes of 0.1 mM aqueous $HAuCl_4$ at initial pH of (A) 11.9 and (B) 4.8, respectively.

adjusted to two different extremes (Figure 6). When the synthesis is conducted in an alkaline solution with an initial pH

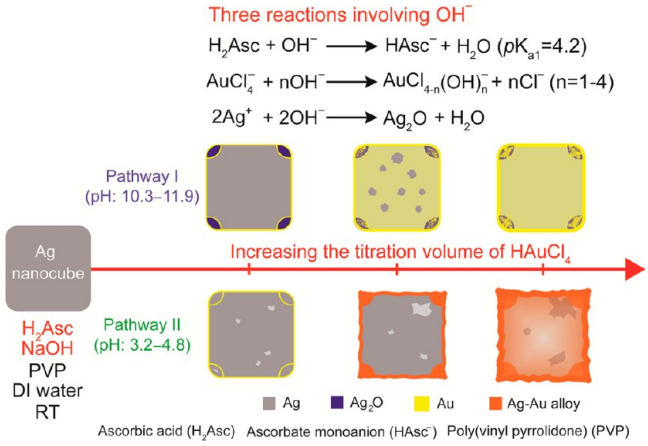

Figure 6. Schematic illustration of two pathways proposed to account for the formation of different types of Ag−Au bimetallic nanocrystals under alkaline and acidic conditions, respectively.

in the range of 10.3−11.9, galvanic replacement can still occur between the Ag nanocubes and the first few drops of aqueous $HAuCl_4$. The oxidation and dissolution of Ag atoms are initiated from the corners due to their lower reactivity than the atoms situated on the edges and side facets. The released Ag^+ ions immediately react with the surrounding OH^- ions to generate Ag_2O patches that ultimately cover the entire {111} facets at the corner sites. The Ag_2O patches can protect the underlying Ag atoms from further oxidation, so the galvanic reaction will cease shortly after it is initiated. From this point, the added $HAuCl_4$ is mostly converted to $AuCl(OH)_3^-$ and $Au(OH)_4^-$ through neutralization and ligand exchange with OH^- ions. These two species have lower reduction potentials than $AuCl_4^-$, helping suppress the galvanic replacement reaction. As a result, Au atoms are mainly produced through the chemical reduction by $HAsc^-$, followed by their preferential deposition on the edges of the nanocubes. As the synthesis proceeds with the introduction of more $HAuCl_4$, the side faces of nanocubes are also covered by Au atoms through direct deposition or surface diffusion from the edges. Because of the presence of oxide patches and therefore increase in nucleation energy barrier,[28] the Au atoms should not be directly deposited on the corners. As shown in Figure S4, we still observed the presence of Au at the corner sites of a nanocube. It is possible that surface diffusion could transport Au atoms from edges to corners, generating an ultrathin layer on top of the Ag_2O patches. Collectively, the final products are Ag@Au core−shell nanocubes with their corners covered by Ag_2O patches and then ultrathin Au layers. When the Ag_2O patches are removed with an acid to lift off the Au deposited on the Ag_2O regions, followed by selective etching of the Ag cores by H_2O_2, the core−shell nanocubes evolve into Au-based nanoboxes with well-defined openings at the corner sites.

If the synthesis is conducted in an acidic solution with an initial pH in the range of 3.2−4.8, the reduction power of H_2Asc will be compromised due to a reduced concentration for $HAsc^-$. On the other hand, the titrated $HAuCl_4$ will dissociate into H^+ and $AuCl_4^-$, followed by the evolution of $AuCl_4^-$ into $AuCl_3(OH)^-$ and $AuCl_2(OH)_2^-$ through ligand exchange. In this case, the Au(III) species can be reduced by both the Ag nanocubes and $HAsc^-$ through galvanic replacement and chemical reduction, respectively. The galvanic reaction tends to occur randomly from any site on a Ag nanocube, while the resultant Au atoms are preferentially deposited on the edges. Because one Au atom is produced at the expenses of three Ag atoms during the galvanic reaction between Au(III) and Ag, a pit will be generated on the surface of a nanocube. As the titration volume of $HAuCl_4$ is increased, the Ag^+ ions will be continuously released from the Ag nanocube, further enlarging the pit. At the same time, the released Ag^+ ions and Au(III) species can both be reduced by $HAsc^-$ to generate Ag and Au atoms, respectively, followed by their codeposition on the edges. Some of these atoms can migrate to the corners through surface diffusion, transforming the Ag nanocube into a Ag@Ag−Au core-frame nanocube with cavities in the interior. As more $HAuCl_4$ is added, the cavity will be enlarged and the Ag and Au atoms resulting from the coreduction will be continuously deposited on the edges and corners, followed by their diffusion to side faces. At the end, Ag@Ag−Au hollow nanocubes with concave side faces are formed. When the Ag cores are selectively removed through wet etching with H_2O_2, the nanocubes evolve into Au−Ag nanocages with pores on the side faces.

To further support our argument, we compared the standard reduction potentials of Ag^+, Au^{3+}, and H_2Asc at different pH values. Figure S5 plots their reduction potentials as a function of pH by taking their values from the literature.[22] As the pH is increased from 2 to 12, the reduction potential of Au(III)/Au(0) gradually decreases due to the transformation from $AuCl_4^-$ to $Au(OH)_4^-$. In contrast, there is little change in the reduction potential of Ag(I)/Ag(0) (0.80 V vs SHE) up to pH = 6.3. As a result, the driving force for the galvanic replacement between Au(III) and Ag(0) should decrease as the pH is

DOI: 10.1021/acs.chemmater.7b00575
Chem. Mater. XXXX, XXX, XXX−XXX

increased. It is worth mentioning that the increase in pH can neutralize more H_2Asc into $HAsc^-$, ultimately accelerating the reduction kinetics for the Au(III) precursor. As a result, the Au(III) precursor will be reduced primarily by $HAsc^-$ rather than the Ag nanocubes under the alkaline condition. We have also systematically studied and compared the extents of galvanic replacement in the absence or presence of NaOH (with no involvement of H_2Asc in both cases) at initial pH of 4.3 and 11.4, respectively. Specifically, we titrated different volumes of $HAuCl_4$ into the aqueous suspension of Ag nanocubes in the presence of PVP only and waited for 10 min before collecting both the solid and supernatant by centrifugation to determine the Ag and Au contents by ICP-MS. As shown in Figure S6, in the absence of NaOH and at an initial pH of 4.3, the Au content in the solid products increased linearly with the volume of $HAuCl_4$ titrated into the reaction solution. At each titration volume, the Au(III) ions remaining in the supernatant was essentially zero. These data suggest that the added $HAuCl_4$ was completely reduced by the Ag nanocubes via the galvanic replacement reaction. In comparison, in the presence of NaOH at pH = 11.4, only 50% of the titrated Au(III) precursor was converted to Au atoms for their deposition on the Ag nanocubes, which indicated that the galvanic replacement reaction was significantly retarded. At an initial pH of 11.4, the added $AuCl_4^-$ is quickly converted to $AuCl(OH)_3^-$ and $Au(OH)_4^-$, both with lower reduction potentials than $AuCl_4^-$, making the galvanic reaction with Ag more difficult. Additionally, any Ag^+ ions released from the Ag nanocubes will react with OH^- for the generation of Ag_2O on the surface of a Ag nanocube, further helping inhibit the galvanic reaction.

We assume that the $HAuCl_4$ precursor titrated into the aqueous suspension of Ag nanocubes should be immediately neutralized by OH^- to yield $AuCl_4^-$ before it further undergoes ligand exchange to generate a mixture of $AuCl(OH)_3^-$ and $Au(OH)_4^-$ at pH > 10.[21] To fully understand the role of ligand exchange between Cl^- and OH^- in affecting the deposition of Au on Ag nanocubes, we performed another control experiment. In this case, we premixed 0.03 mL of $HAuCl_4$ (10 mM) with 0.1 mL of NaOH (0.2 M) in 2.87 mL of water to obtain a 0.1 mM Au(III) precursor solution with pH = 11.5. We then titrated the Au(III) precursor solution into an aqueous suspension of Ag nanocubes in the presence of H_2Asc, NaOH, and PVP at an initial pH of 11.9. Figure S7A shows TEM image of the products obtained at a titration volume of 0.8 mL. The particles were essentially the same as those shown in Figure 3E. However, upon the removal of Ag cores by H_2O_2 etching, the resultant nanoboxes shown in Figure S7B are different from those shown in Figure 3F. In this case, we observed a significant population of nanoboxes without openings at the corers. This result clearly shows the difference between $AuCl_4^-$ and $Au(OH)_4^-$, which suggests that the conversion between them through the ligand exchange with OH^- was not instantaneous. Interestingly, the initial involvement of galvanic replacement between $AuCl_4^-$ and the Ag atoms located at the corners of nanocubes was instrumental to the formation of Au-based nanoboxes with well-defined openings at the corners.

CONCLUSIONS

We have demonstrated the role of hydroxide in controlling the deposition of Au atoms on Ag nanocubes for the generation of Ag−Au bimetallic nanocubes with different structures. When we conduct the synthesis in an alkaline solution with an initial pH in the range of 10.3−11.9, H_2Asc is neutralized by OH^- to give $HAsc^-$, a strong reducing agent. The $HAuCl_4$ precursor titrated into the aqueous suspension of Ag nanocubes is quickly neutralized by OH^- to yield $AuCl_4^-$. The $AuCl_4^-$ then undergo galvanic replacement with the Ag atoms situated at the corners of a nanocube to initiate the deposition of Au atoms at the edges. Because of the presence of OH^- ions, the released Ag^+ ions are immediately converted to Ag_2O, generating oxide patches at the corners. As such, the galvanic reaction will be terminated shortly after it is initiated to prevent further dissolution of Ag from the nanocube. Afterward, $AuCl_4^-$ is progressively converted into $AuCl(OH)_3^-$ and $Au(OH)_4^-$ through ligand exchange, and Au atoms are continuously produced through the reduction by $HAsc^-$, followed by their deposition on the edges and side faces for the formation of a Ag@Au core−shell nanocube, with some Au deposition at the corners on top of Ag_2O. Selective removal of the Ag cores generates Au-based cubic nanoboxes with well-defined openings at the corners. When the initial pH of reaction solution was adjusted in the range of 3.2−4.8, the titrated $HAuCl_4$ precursor actually exists as a mixture of $AuCl_4^-$, $AuCl_3(OH)^-$ and $AuCl_2(OH)_2^-$ in the reaction solution. These Au(III) species will be reduced through both the galvanic reaction with Ag nanocubes and the chemical reduction by $HAsc^-$. Additionally, the released Ag^+ ions from the Ag nanocubes can be reduced by $HAsc^-$ to generate Ag atoms, followed by their codeposition with Au atoms on the edges of nanocubes. The codeposited Ag and Au atoms can spread to the corners and side faces by surface diffusion, eventually leading to the formation of Ag@Ag−Au concave nanocubes with hollow interiors as the volume of the titrated $HAuCl_4$ is increased. Selective removal of the Ag cores leads to the formation of nanoframes or nanocages with poorly defined pores on the side faces. We believe this mechanistic study of Au deposition on colloidal Ag nanocrystals can provide guidance for the rational design of Ag-based bimetallic nanocrystals involving metals such as Au, Pd, and Pt for the fabrication of novel functional nanomaterials.

ASSOCIATED CONTENT

Supporting Information

The Supporting Information is available free of charge on the ACS Publications website at DOI: 10.1021/acs.chemmater.7b00575.

Structure of ascorbic acid; SEM and TEM images of Ag nanocubes; pH values as function titration volume of $HAuCl_4$; STEM and EDS images of Ag@Au core−shell nanocube; reduction potentials of Ag(I), Au(III), and ascorbic acid as a function of pH; ICP-MS data; TEM images of Ag@Au nanocubes before and after etching by H_2O_2 (PDF)

AUTHOR INFORMATION

Corresponding Author

*E-mail: dong.qin@mse.gatech.edu.

ORCID

Dong Qin: 0000-0001-5206-5912

Notes

The authors declare no competing financial interest.

DOI: 10.1021/acs.chemmater.7b00575
Chem. Mater. XXXX, XXX, XXX−XXX

■ ACKNOWLEDGMENTS

This work was supported in part by the National Science Foundation (CHE-1412006), start-up funds from Georgia Tech, and a 3M nontenured faculty award. Part of the work was performed in the Institute of Electronics and Nanotechnology (IEN) at the Georgia Institute of Technology. We thank J. Ahn for performing the ICP-MS analyses.

■ REFERENCES

(1) Willets, K. A.; Van Duyne, R. P. Localized Surface Plasmon Resonance Spectroscopy and Sensing. *Annu. Rev. Phys. Chem.* **2007**, *58*, 267−297.
(2) Haes, A. J.; Haynes, C. L.; McFarland, A. D.; Schatz, G. C.; Van Duyne, R. P.; Zou, S. Plasmonic Materials for Surface-Enhanced Sensing and Spectroscopy. *MRS Bull.* **2005**, *30*, 368−375.
(3) Rycenga, M.; Cobley, C. M.; Zeng, J.; Li, W.; Moran, C. H.; Zhang, Q.; Qin, D.; Xia, Y. Controlling the Synthesis and Assembly of Silver Nanostructures for Plasmonic Applications. *Chem. Rev.* **2011**, *111*, 3669−3712.
(4) McLellan, J. M.; Li, Z.-Y.; Siekkinen, A. K.; Xia, Y. The SERS Activity of a Supported Ag Nanocube Strongly Depends on Its Orientation Relative to Laser Polarization. *Nano Lett.* **2007**, *7*, 1013−1017.
(5) Haes, A. J.; Van Duyne, R. P. A Nanoscale Optical Biosensor: Sensitivity and Selectivity of an Approach Based on the Localized Surface Plasmon Resonance Spectroscopy of Triangular Silver Nanoparticles. *J. Am. Chem. Soc.* **2002**, *124*, 10596−10604.
(6) Xia, X.; Zeng, J.; McDearmon, B.; Zheng, Y.; Li, Q.; Xia, Y. Silver Nanocrystals with Concave Surfaces and Their Optical and Surface-Enhanced Raman Scattering Properties. *Angew. Chem.* **2011**, *123*, 12750−12754.
(7) Xia, Y.; Xiong, Y.; Lim, B.; Skrabalak, S. E. Shape-Controlled Synthesis of Metal Nanocrystals: Simple Chemistry Meets Complex Physics? *Angew. Chem., Int. Ed.* **2009**, *48*, 60−104.
(8) Pastoriza-Santos, S.; Liz-Marzán, L. M. Colloidal Silver Nanoplates. State of the Art and Future Challenges. *J. Mater. Chem.* **2008**, *18*, 1724−1737.
(9) Millstone, J. E.; Hurst, S. J.; Metraux, G. S.; Cutler, J. I.; Mirkin, C. A. Colloidal Gold and Silver Triangular Nanoprisms. *Small* **2009**, *5*, 646−664.
(10) Linic, S.; Christopher, P.; Ingram, D. B. Plasmonic-Metal Nanostructures for Efficient Conversion of Solar to Chemical Energy. *Nat. Mater.* **2011**, *10*, 911−921.
(11) Christopher, P.; Xin, H.; Linic, S. Visible-Light-Enhanced Catalytic Oxidation Reactions on Plasmonic Silver Nanostructures. *Nat. Chem.* **2011**, *3*, 467−472.
(12) McLellan, J. M.; Siekkinen, A.; Chen, J.; Xia, Y. Comparison of the Surface-Enhanced Raman Scattering on Sharp and Truncated Silver Nanocubes. *Chem. Phys. Lett.* **2006**, *427* (1−3), 122−126.
(13) Christopher, P.; Linic, S. Engineering Selectivity in Heterogeneous Catalysis: Ag Nanowires as Selective Ethylene Epoxidation Catalysts. *J. Am. Chem. Soc.* **2008**, *130* (34), 11264−11265.
(14) Yang, Y.; Liu, J.; Fu, Z.; Qin, D. Galvanic Replacement-Free Deposition of Au on Ag for Core-Shell Nanocubes with Enhanced Chemical Stability and SERS Activity. *J. Am. Chem. Soc.* **2014**, *136*, 8153−8156.
(15) Zhang, J.; Winget, S. A.; Wu, Y.; Su, D.; Sun, X.; Xie, Z. X.; Qin, D. Ag@Au Concave Cuboctahedra: A Unique Probe for Monitoring Au-Catalyzed Reduction and Oxidation Reactions by Surface-Enhanced Raman Spectroscopy. *ACS Nano* **2016**, *10*, 2607−2616.
(16) Li, J.; Sun, X.; Qin, D. Ag-Enriched Ag-Pd Bimetallic Nanoframes and Their Catalytic Properties. *ChamNanoMat* **2016**, *2*, 494−7499.
(17) Li, J.; Liu, J.; Yang, Y.; Qin, D. Bifunctional Ag@Pd-Ag Nanocubes for Highly Sensitive Monitoring of Catalytic Reactions by Surface-Enhanced Raman Spectroscopy. *J. Am. Chem. Soc.* **2015**, *137*, 7039−7042.
(18) Li, J.; Wu, Y.; Sun, X.; Liu, J.; Winget, S. A.; Qin, D. A Dual Catalyst with SERS Activity for Probing Stepwise Reduction and Oxidation Reactions. *ChamNanoMat* **2016**, *2*, 786−790.
(19) Sun, X.; Qin, D. Co-Titration of $AgNO_3$ and $HAuCl_4$: A New Route to the Synthesis of Ag@Ag−Au Core−frame Nanocubes with Enhanced Plasmonic and Catalytic Properties. *J. Mater. Chem. C* **2015**, *3*, 11833−11841.
(20) Du, J.; Cullen, J. J.; Buettner, G. R. Ascorbic Acid: Chemistry, Biology, and the Treatment of Cancer. *Biochim. Biophys. Acta, Rev. Cancer* **2012**, *1826*, 443−457.
(21) Wang, S.; Qian, K.; Bi, X.; Huang, W. Influence of Speciation of Aqueous $HAuCl_4$ on the Synthesis, Structure, and Property of Au Colloids. *J. Phys. Chem. C* **2009**, *113*, 6505−6510.
(22) Goia, D. V.; Matijević, E. Tailoring the Particle Size of Monodispersed Colloidal Gold. *Colloids Surf., A* **1999**, *146*, 139−152.
(23) Hickling, A.; Taylor, D. The Anodic Behaviour of Metals. Part IV. Silver. *Discuss. Faraday Soc.* **1947**, *1*, 277−285.
(24) Zhang, Q.; Li, W.; Wen, L. P.; Chen, J.; Xia, Y. Facile Synthesis of Ag Nanocubes of 30 to 70 nm in Edge Length with CF_3COOAg as a Precursor. *Chem. - Eur. J.* **2010**, *16*, 10234−10239.
(25) Yang, Y.; Zhang, Q.; Fu, Z.-W.; Qin, D. Transformation of Ag Nanocubes into Ag−Au Hollow Nanostructures with Enriched Ag Contents to Improve SERS Activity and Chemical Stability. *ACS Appl. Mater. Interfaces* **2014**, *6*, 3750−3757.
(26) Sun, X.; Kim, J.; Gilroy, K. D.; Liu, J.; König, T. A. F.; Qin, D. Gold-Based Cubic Nanoboxes with Well-Defined Openings at the Corners and Ultrathin Walls Less Than Two Nanometers Thick. *ACS Nano* **2016**, *10*, 8019−8025.
(27) Chen, J.; McLellan, J. M.; Siekkinen, A.; Xiong, Y.; Li, Z.-Y.; Xia, Y. Facile Synthesis of Gold-Silver Nanocages with Controllable Pores on the Surface. *J. Am. Chem. Soc.* **2006**, *128*, 14776−14777.
(28) Venables, J. A. *Introduction to Surface and Thin Film Processes*; Cambridge University Press: Cambridge, U.K., 2000.

DOI: 10.1021/acs.chemmater.7b00575
Chem. Mater. XXXX, XXX, XXX−XXX